Nelson *et al. Energy Mater* 2024;4:400064
DOI: 10.20517/energymater.2024.04

Energy Materials

Article

Open Access

Check for updates

Creating value added nano silicon anodes from end-of-life photovoltaic modules: recovery, nano structuring, and the impact of ball milling and binder on its electrochemical performance

Akhil Nelson[1], Srikanth Mateti[1], Ying Chen[1,*], Neeraj Sharma[2], Qi Han[3], Md Mokhlesur Rahman[1,*]

[1]Institute for Frontier Materials, Deakin University, Waurn Ponds, VIC 3216, Australia.
[2]School of Chemistry, University of New South Wales, Sydney, NSW 2052, Australia.
[3]School of Science, STEM College, RMIT University, Melbourne, VIC 3000, Australia.

***Correspondence to:** Dr. Ying Chen, Institute for Frontier Materials, Deakin University, Waurn Ponds, VIC 3216, Australia. E-mail: ian.chen@deakin.edu.au; Dr. Md Mokhlesur Rahman, Institute for Frontier Materials, Deakin University, Waurn Ponds, VIC 3216, Australia. E-mail: m.rahman@deakin.edu.au

How to cite this article: Nelson A, Mateti S, Chen Y, Sharma N, Han Q, Rahman MM. Creating value added nano silicon anodes from end-of-life photovoltaic modules: recovery, nano structuring, and the impact of ball milling and binder on its electrochemical performance. *Energy Mater* 2024;4:400064. https://dx.doi.org/10.20517/energymater.2024.04

Received: 17 Jan 2024 **First Decision:** 27 Mar 2024 **Revised:** 8 Apr 2024 **Accepted:** 18 Apr 2024 **Published:** 27 Jun 2024

Academic Editors: Yuping Wu, Félix A. Lopez **Copy Editor:** Fangyuan Liu **Production Editor:** Fangyuan Liu

Abstract

Recovery of silicon from end-of-life photovoltaic (PV) modules, purification, conversion to nano silicon (nano-Si), and subsequent application as an anode in lithium-ion batteries is challenging but can significantly influence the circular economy. Currently, a complete technology consisting of cross-contamination-free recovery of silicon wafers from end-of-life PV modules, a low-cost environmentally friendly purification process of the recovered PV silicon, a high yield conversion process of the recovered PV silicon into nano-Si, and its subsequent application in lithium-ion batteries is unavailable. This study provides a complete package including cross-contamination-free recovery, economical purification, reliable conversion to nano-Si, and efficient application of the end-of-life PV nano-Si in lithium-ion batteries. Hydrofluoric acid-free recovery and purification processes are demonstrated which can deliver large quantities of high-purity (≥ 99) silicon. In addition, the subsequent ball milling process produces very distinct nano-Si with different shapes and sizes. This study also creates a very effective nano-Si anode through in-situ crosslinking of water-soluble carboxymethyl cellulose and poly (acrylic acid) precursors. The integration of distinct PV nano-Si and water-soluble carboxymethyl cellulose-poly (acrylic acid) crosslink binder opens distinct possibilities to develop silicon-based practical anode for next generation low-cost lithium-ion batteries to power cell phones to electric vehicles.

Keywords: End-of-life photovoltaic module, nano silicon, crosslink binder, silicon anode, lithium-ion batteries

INTRODUCTION

Photovoltaic (PV) systems are the most appealing power generation systems with a negligible impact on air quality and climate change compared to the traditional power generation systems[1,2]. It has been demonstrated that they can reduce electricity generation to the emission of 0.53 kg CO_2/kWh[3]. Therefore, the demand of PV module installations is expanding rapidly which will also lead to an increase in the volume of end-of-life (EoL) PV waste shortly. It is projected that around 78 million tons of PV waste will be generated by 2050, which will eventually create serious environmental hazards if such massive waste ends up in landfills[4,5]. It is important to note that PV waste contains a wide range of elements, including silicon (Si), aluminum (Al), silver (Ag), copper (Cu), lead (Pb), cadmium (Cd), selenium (Se), phosphorous (P), boron (B), and barium (Ba). Many of these elements are hazardous and can easily leach and mix with soil and groundwater, creating major threats to the survival of living beings, including wildlife, livestock, and humans[4,6,7]. Thus, the expansion of PV technology generates a challenge of EoL management of PV modules because the average lifespan of a crystalline silicon (c-Si) PV module is about 25-30 years[8,9].

A PV module comprises six main components: PV cells, thick tempered glass, aluminum frame, encapsulant, back-sheet, and junction box. A typical c-Si PV module contains approximately 75% tempered glass, 10% polymer (encapsulant and back sheet foil), 8% Al (mostly the frame), 5% Si (solar cells or PV cells), and 2% other metals/elements[8,10]. Based on the PV module construction, it is anticipated that PV materials, especially tempered glass, polymer, aluminum, silicon (solar or PV cells), and a small amount of other metals, can be recovered from EoL PV modules [Supplementary Figure 1] and reused to support the circular economy which is an ideal sustainability goal for the PV industry[11-13]. At present, many countries, including Europe, Japan, Norway, the USA, and Australia, are focusing on research into solar module recycling. Currently, the most common methods for recycling c-Si PV modules are based on physical/mechanical and chemical processes. Although chemical processes can utilize various chemicals to recover Si from PV cells/wafers, hydrofluoric (HF) acid is the most common solvent used to separate Si[14-16]. HF is highly toxic and corrosive and not an environmentally friendly chemical. In addition, most reported recycling techniques are complicated, multistep, time-consuming, low-yield, and most importantly, the recovered materials are cross-contaminated which require additional processes to purify.

In this study, an advanced recycling process has been adopted to recover PV cells/wafers from EoL PV modules. Additionally, an environmentally friendly, low-cost purification process has been established, reclaiming high-purity Si (≥ 99) from PV cells with a recovery rate of around 80%. For efficient application, the obtained recycled Si needs to be nanosized which requires physical modification. Among various procedures, mechanical ball milling is recognized as a promising practical technique for preparing nanoparticles in large quantities. Herein, planetary ball milling is adopted to reduce particle size of the recovered PV Si. We have carefully studied the connection between milling time, the structure of the PV-derived nano-Si, and the role of binders for battery performance. We anticipate that optimizing the ball milling time, gaining a better understanding of the nano structuring of PV-derived Si, and exploring the role of the binder and its relationship with battery performance will provide critical information to aid in the design and fabrication of practical silicon anodes. The obtained PV-derived nano-Si prepared through 3h milling shows very distinct properties with different shapes and sizes (between 30-200 nm) and can be a contender (in terms of cost and properties) to the commercial nano-Si available in the market. The production cost of PV recycled nano-Si ($600-700/Kg) is much cheaper than that of commercially available Sigma-Aldrich nano-Si ($45,000-50,000/Kg).

EXPERIMENTAL

Purification of the recovered PV cells/wafers

Removal of aluminum impurity

A suitable amount of the recovered PV cells/wafers from EoL PV modules and potassium hydroxide (KOH) with moderate concentration were loaded into a laboratory screw cap glass bottle. The mixture was heat treated at 80 °C for 15 min under vigorous stirring. The aluminum (Al) metal impurities were dissolved in the alkaline solution, and the PV Si formed sediments. The mixture was then washed thoroughly with de-ionized (DI) water several times to remove all Al and other dissolved impurities.

Removal of silver (Ag), lead (Pb), and antireflective coating layer (Si_3N_4)

After Al removal, a suitable amount of the recovered PV cells/wafers were loaded into a laboratory screw cap glass bottle and mixed with nitric acid (HNO_3) and 85% concentrated phosphoric acid (H_3PO_4). The mixture was then heat treated under vigorous stirring. The solution was washed thoroughly with DI water several times. This process was undertaken to leach out dissolved Ag, Pb, and Si_3N_4. HNO_3 is responsible for removing Ag and Pb, whereas H_3PO_4 is employed to remove the antireflective coating layer of Si_3N_4. Upon successful leaching, the recovered PV Si was dried under vacuum at 110 °C for 24 h.

Materials characterization

X-ray diffraction (XRD) data were collected on a PANalytical X'Pert Pro Instrument, Panalytical Aeris and MPD diffractometers using Cu radiation. Rietveld refinements were performed using the structural model of Si in *Fd*-3*m* space group symmetry with the XRD data using General Structure Analysis System II (GSASII)[17,18]. Each refinement involved six background terms: zero, lattice parameter, profile terms U, V, W and Lorentzian Y, and the atomic displacement parameter of Si. X-ray fluorescence (XRF) was carried out on PANalytical Axios Advanced WDXRF using an end window Rh tube operated at 4 kW. For the determination of nitrogen (N), Elementar varioMACRO cube (CHNS) methodology (varioMACRO cube, Langenselbold, Germany) was used. An Agilent-Japan 7900 ICP-MS (Inductively coupled plasma mass spectroscopy) determined impurity concentration in the samples. X-ray photoemission spectroscopy (XPS) was employed using a Thermo Scientific K-Alpha instrument (monochromatic Al Kα radiation). Morphologies of the samples were examined using scanning electron microscopy (SEM, Carl Zeiss Supra 55 VP Instrument). Transmission electron microscopy (TEM) analysis was performed on a JEOL JEM 2100F instrument operated at 200 kV with a JEOL-Energy Dispersive X-ray Spectroscopy (EDS) detector and the JEOL EDS software analysis system.

Electrochemical characterization

For electrochemical performance evaluation, powder samples were mixed with Super-P Li carbon black and a binder, carboxymethyl cellulose (CMC), with a weight ratio of 60:20:20 in a solvent (distilled water). The slurry was spread onto Cu foil substrates, and these coated electrodes were dried in a vacuum oven at 100 °C for 24 h. To evaluate the binder effect, a weight ratio of 60:(10:10):20 (powder: binder (CMC: poly (acrylic acid) (PAA)): Super P Li) was used for preparing electrode slurry for the 3 h sample. The obtained slurry was spread onto Cu foil substrates, and these coated electrodes were dried in a vacuum oven at 150 °C for 2 h and then 100 °C for 24 h. CR 2032 coin-type cells were assembled in an Ar-filled glove box. The cells were galvanostatically discharged/charged within a voltage range of 0.01-2.0 V using a land battery testing system. Cyclic voltammograms (CV) were recorded using Solartron Analytical electrochemical workstations at a scan rate of 0.1 mV s^{-1}.

RESULTS AND DISCUSSION

Purification of the recovered PV cells/wafers

As Si is the highest cost component among all parts of a PV module, the recovery of Si/cells from EoL PV modules and their purification for reuse are critical. However, the recovered PV cells contain a wide range of impurities, as confirmed by XRD, SEM-EDS in Figure 1, XRF analysis, and ICP-MS spectroscopy in Table 1. Figure 1A compares XRD peaks between the recovered PV cells and commercial Si available in the market. Although the profiles of the diffraction peaks of the PV cells are well matched with the commercial Si with a cubic crystal system (JCPDS no. 04-014-8844; space group: *Fd*-3*m*; space group number: 227), some peaks were in good agreement with Al (JCPDS: 01-071-4625), confirming the presence of Al in the recovered PV cells. From the construction point of view, PV cells contain not only Al but also trace amounts of other elements or compounds. SEM with corresponding EDS and XRF were carried out on the recycled PV samples, and Figure 1B demonstrates the compositional EDS analysis of the front side (upper face-blue in color) of the PV cells with the insert showing the SEM image. It is evidenced that the front side or upper face of the PV cell is composed of Si (~80 at%), N (~20 at%), and Al (~0.5 at%). No Cd, Ag, B, and Pb were detected. SEM-EDS analysis of the back side (down face) of the PV cell is shown in Figure 1C. EDS analysis shows that the back side (down face-grey in color) of the PV cell is composed of Al (~84 at%) and Si (~16 at%). No Cd, Ag, B, Pb, and N were detected. The presence of N in the front side of the PV cell confirms the existence of an antireflective (AR) coating layer which is commonly made of silicon nitride (Si_3N_4), responsible for the blue color of the cells[10]. In addition, the front side of the PV cell mostly contains Si whereas the back side is mostly Al. However, XRF analysis detects the presence of a trace amount of Ag (5,237 ppm), Cd (25 ppm), and Pb (12 ppm) in the sample. To get more insight about impurities in the sample, ICP-MS spectroscopy was performed and several elements were detected, including Al (102,040), Ag (232.78), V (11.64), Cr (0.58), Co (1.33), As (0.37), Se (0.98), Cd (1.01), Sn (4.70), Sb (3.01), and Pb (6.74) mg/kg, respectively.

To remove the above-mentioned impurities from the recovered PV cells, a chemical leaching process was developed. For this chemical leaching process, four different solvents, including KOH, HNO_3, sulfuric acid (H_2SO_4), and H_3PO_4, were used. Figure 2A shows the XRD patterns of the PV cells after being chemically treated first with 2, 5, and 10 M KOH at 80 °C for 15 min and followed by 2, 5, and 10 M HNO_3 at 80 °C for 15 min. Visual inspection of the XRD patterns indicates that most of the Al peaks disappear (compare Figure 2A and Figure 1A), as further confirmed by SEM-EDS analysis. The presence of a trace amount of Al in the front side of the PV cells still exists even after chemical treatment with KOH (compare Figure 1B and Figure 2B-E). On the other hand, the most Al (~84 at%) in the untreated PV cells is found in the back side of the PV cells [Figure 1C] which is dramatically reduced to 0.3, 0.2, and 0.2 at% when treated with 2, 5, and 10 M KOH [Figure 2F-H], respectively. The front side of the PV cells is fully covered by the AR coating layer of Si_3N_4, which may protect the reaction between KOH and Al. No significant concentration effects (2, 5, and 10 M KOH) on the dissolution of Al is found in this study. Most Al present in the back side of the cells reacts with KOH based on

$$2Al + 2KOH + 6H_2 \rightarrow 2K^+ + 2Al(OH)_4^- + 3H_2 \uparrow \quad (1)$$

After heat treatment of the PV cells with KOH, the samples were washed with DI water several times, and further heat treatment at 80 °C for 15 min was carried out with various concentrations of 2, 5, and 10 M HNO_3 to remove other trace metals. However, it is seen that both KOH and HNO_3 solvents cannot remove the AR coating layer of Si_3N_4 from the front side of the PV cells. Both chemically untreated and treated PV cells (front side) show approximately the same amount of N present in the samples (compare Figure 1B and Figure 2B-E), suggesting the existence of the Si_3N_4 layer in the samples.

Table 1. Comparison of ICP-MS analysis data between recovered PV Si (before purification), purified PV Si, and commercial Si

Samples	Impurities (concentration: mg/Kg)										
	Al	Ag	V	Co	As	Se	Cd	Pb	Cr	Sb	Sn
Recovered PV silicon	102,040	232.78	11.64	1.33	0.37	0.98	1.01	6.74	0.58	3.01	4.70
Purified PV silicon	57.67	1.99	0.16	0.01	0.04	0.01	BDL	0.16	BDL	0.17	0.27
Sigma-Aldrich silicon	392.67	3.01	4.46	0.56	0.09	0.16	0.01	0.52	-	0.14	0.30

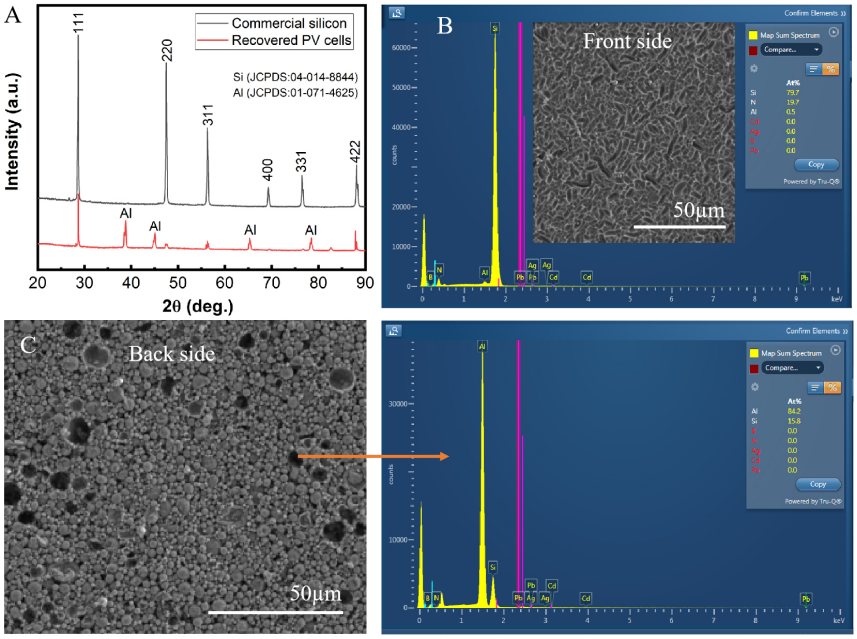

Figure 1. Initial compositional analysis of the recovered PV cells (before purification): (A) XRD patterns of the commercial Si and the recovered PV cells; and (B and C) SEM-EDS analysis of the recovered PV cells: (B) Front side (upper face) and (C) Back side (down face).

The PV cell sample treated with 10 M KOH and 10 M HNO_3 was selected to conduct further heat treatment with concentrated 98% H_2SO_4 to remove the AR coating layer of Si_3N_4. Notably, it appears that using 10 M KOH and 10 M HNO_3 is not necessary, but for this study, it was chosen as an "extreme" case. Following the H_2SO_4 treatment, PV samples were heated for 1 h under temperatures of 100, 150 and 200 °C, respectively. A significant temperature effect is observed among the post-treated samples, especially an increase in the XRD peak intensity with rising temperatures. This suggests higher crystallinity of the sample treated at 200 °C. However, H_2SO_4 is found to be ineffective for the removal of the Si_3N_4 coating layer from PV cells. All three samples treated with 10 M KOH + 10 M HNO_3 + 98% H_2SO_4 at 100, 150 and 200 °C remain blue [Supplementary Figure 2], indicating the presence of Si_3N_4 in the sample. As H_2SO_4 is inefficient in dissolving the AR coating layer of Si_3N_4, it was replaced by H_3PO_4. H_3PO_4 and heat treatment of the PV samples was carried out for 1h under temperatures of 100, 150 and 200 °C, respectively. Supplementary Figure 3A compares the XRD patterns of these samples with commercial bulk Si. Interestingly, heat treatment with H_3PO_4 leads to PV-derived Si featuring significantly less crystallinity and possibly an amorphous Si sample, as many peaks reduce in intensity and disappear. However, the obvious blue color in the PV cells vanishes with increasing treatment temperature (compare Supplementary Figure 3B-D and Supplementary Figure 2C-E), suggesting that H_3PO_4 can dissolve the Si_3N_4 coating layer.

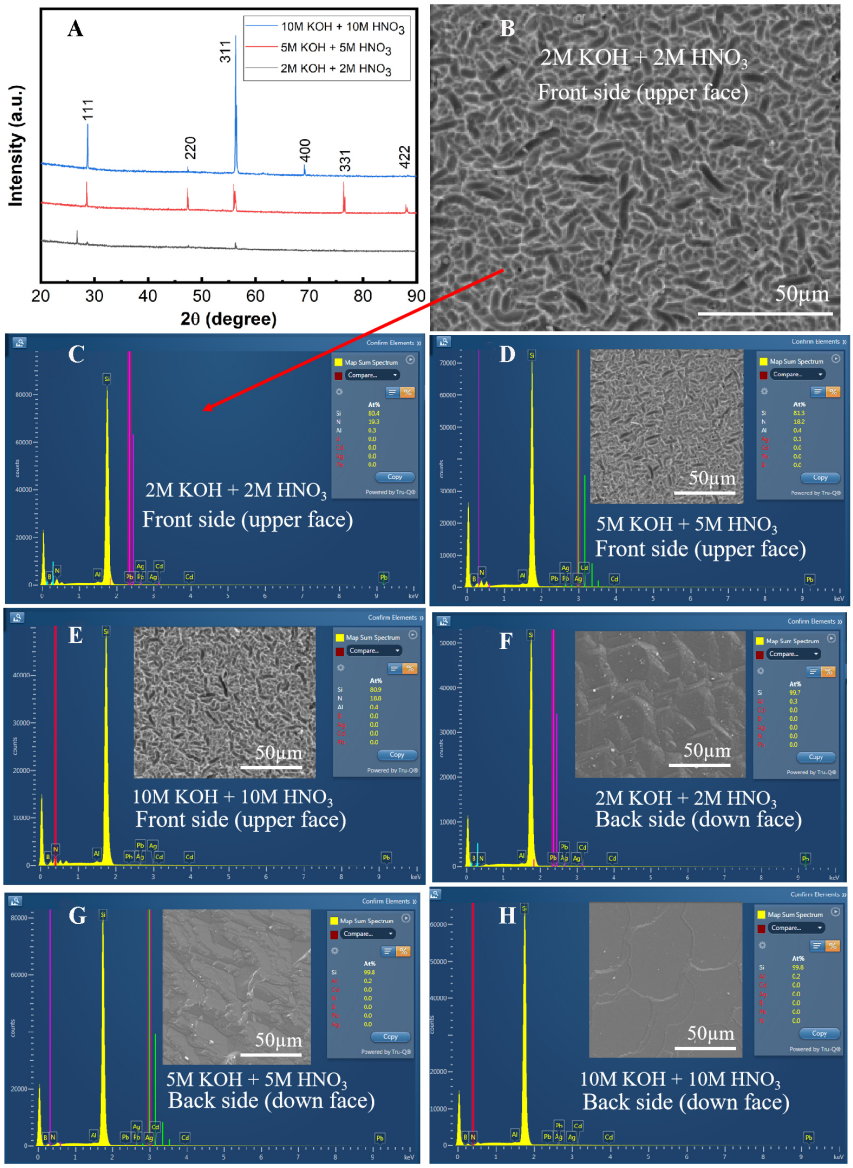

Figure 2. Purification of recycled PV cells with various concentrations of 10, 5, and 2M KOH and 10, 5, and 2M HNO_3 solution at 80 °C for 15 min: (A) X-ray diffraction patterns of the PV cells after chemical treatment; and (B-H) SEM images and corresponding spectra of the PV cells (both front side-upper face and back side-down face).

To achieve higher Si yield with a lower cost and reasonable crystallinity, it is thus required to optimize purification processes. It is demonstrated that the acid mixture of 10 M HNO_3 and 85% H_3PO_4 effectively removes the majority of the impurities, including the Si_3N_4 coating layer. It is observed from XRD patterns [Figure 3A] that the purified PV-derived Si is crystalline and matches the commercial Si. The blue color of the PV cells vanished after being heat treated with a mixture of 10 M HNO_3 and 85% H_3PO_4 acid solvent at 150 °C [Figure 3B]. During this acid dissolution step, 10 M HNO_3 can react with Ag and Pb (if they exist in the PV cells) which are leached out presumably according to equations (2-4). As HNO_3 is a highly oxidizing agent, the Al removal with KOH solution is conducted first. In this way, the formation of a passivation layer of Al_2O_3 with a reaction between Al and HNO_3 is prevented.

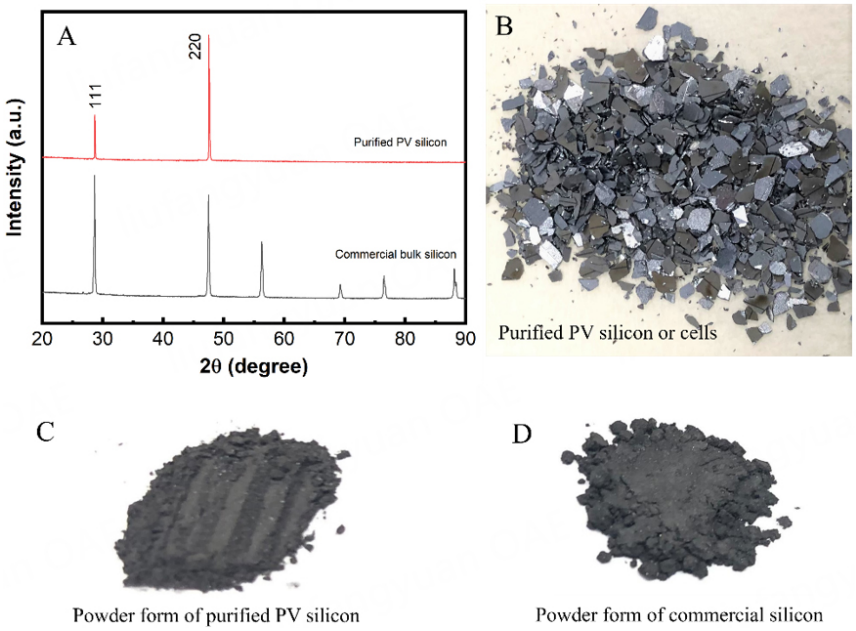

Figure 3. Purification of recycled PV cells with 10 M KOH and an acid mixture of 10 M HNO_3-85% H_3PO_4 at 150 °C for 1 h: (A) XRD patterns of the commercial bulk Si and purified PV Si; (B) Photograph of the purified PV cells; and (C and D) Photographs of purified PV Si powder and commercial Si powder.

$$\text{Leaching of Ag: } Ag + 2HNO_3 \rightarrow AgNO_3 + H_2O + NO_2 \uparrow \quad (2)$$

$$\text{Leaching of Pb: } Pb + 2HNO_3 \rightarrow PbO + H_2O + 2NO_2 \uparrow \quad (3)$$

$$PbO + 2HNO_3 \rightarrow Pb(NO_3)_2 + H_2O \quad (4)$$

The use of 85% H_3PO_4 is responsible for leaching out the Si_3N_4 coating layer. The dissolution reaction of Si_3N_4 in 85% H_3PO_4 can be determined by equation (5). In this dissolution reaction, Si_3N_4 is first hydrated by H_2O and then attacked by H_3PO_4 with simultaneous breaking of Si-N bond and Si-OH group formation[14,19-21].

$$3Si_3N_4 + 4H_3PO_4 + 27H_2O \rightarrow 4\,(NH_4)_3PO_4 + H_2SiO_3 \quad (5)$$

Additionally, no color difference is observed between the powder form of the purified PV-derived Si and commercial Si (compare Figure 3C and Figure 3D), suggesting complete removal of Si_3N_4 from PV-derived Si. To evaluate the quality of the purified PV-dervied Si, ICP-MS analysis was further conducted [Table 1]. The ICP-MS data demonstrates that this purification process is very effective to significantly remove impurities from PV-derived Si. The obtained PV-derived Si appears to be high quality than commercially available Si in the market.

Nano structuring and ball milling effect on the purified PV silicon

The obtained purified PV Si needs to be nanosized for its efficient application in battery technologies. Ball milling of bulk purified PV Si was carried out to evaluate the influence of milling time on the morphology, structure, and subsequent performance. Figure 4A compares XRD data to study the crystal structure and phase purity between various ball-milled PV nano-Si prepared by 1, 3, and 9 h milling, respectively. In all

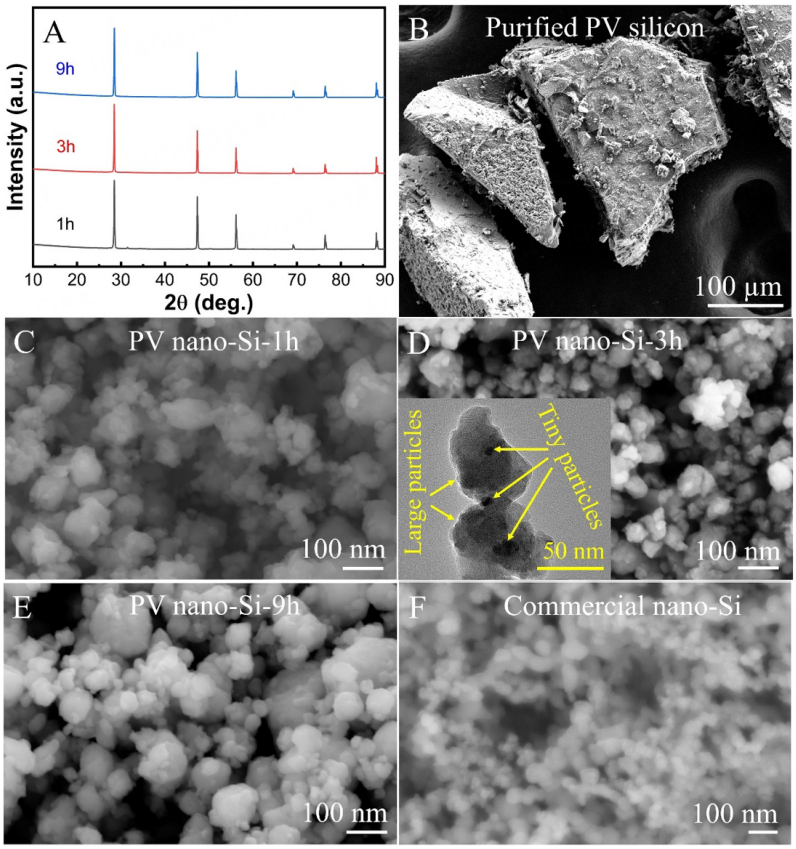

Figure 4. (A) XRD patterns of the ball-milled PV nano-Si with various milling times (1, 3 and 9 h) and (B-F) SEM images: (B) Purified PV Si (before ball milling); (C) PV nano-Si-1h; (D) PV nano-Si-3h with inset TEM bright field image; (E) PV nano-Si-9h; and (F) Commercial nano-Si (Sigma-Aldrich).

ball-milled cases, the major crystalline product is Si adopting the cubic *Fd*-3*m* space group symmetry. Rietveld refinements illustrate similar lattice parameters across the milled series, varying by less than 0.0015 Å, as seen in Supplementary Table 1 and the Rietveld-refined fits in Supplementary Figure 4. The 1 h sample clearly shows the presence of additional crystalline impurities in the patterns (see Supplementary Figure 4B). These impurities dramatically decrease with ball milling time. The particle size distribution using Scherrer analysis suggests an increase from 1 to 3 h followed by a decrease at 9 h ball milling. The 3 h sample showed the largest lattice parameter and particle size distribution. Figure 4B-E shows SEM images of the samples. The ball-milled PV nano-Si samples consist of agglomerated clusters composed of a wide range of nanoparticles [Supplementary Figure 5]. Ball milling has turned micron size PV Si into nano-Si (compare Figure 4B and Figure 4C-E), and milling time significantly influences the reduction of particle sizes. The 1 h ball-milled sample (denoted as PV nano-Si-1h) shows that the majority of particles are larger than 100 nm whereas the 3 h ball-milled sample (denoted as PV nano-Si-3h) exhibits a larger particle size distribution with different shapes and sizes (between 30-200 nm) (compare Figure 4B and C and Figure 4D) which is in good agreement with the TEM bright-filed image (inset in Figure 4D). In the case of the 9h sample (denoted as PV nano-Si-9h), spherical small particles (mostly < 100 nm) are observed (compare Figure 4C-E by Figure 4E). It is interesting to note that PV nano-Si-3h samples show different shapes and sizes of the particles whereas a more uniform particle size and shape is shown in the commercial nano-Si sample (compare Figure 4D and Figure 4F).

To further justify the quality of the PV nano-Si, X-ray photoelectron spectroscopy (XPS) was conducted on PV nano-Si-3h and commercial nano-Si samples [Figure 5]. The obtained spectra for the PV nano-Si-3h sample display a Si2p peak at ~99.5 eV which is composed of $2p_{3/2}$ and $2p_{1/2}$ because of spin-orbit coupling, corresponding to the bulk Si and a peak at 102.5 eV corresponding to the oxide layer (SiO_2) on the surface of Si nanoparticles [Figure 5A]. The O1s spectrum comprises one major component at ~532.5 eV which could be associated with O environments in the SiO_2 [Figure 5B]. The XPS data presented here for the PV nano-Si sample agrees well with the reported results of Si samples[22-25] and commercial nano-Si [Figure 5C and D]. However, the intensity of the SiO_2 peak for the PV nano-Si-3h sample is much stronger than the peak of the commercial nano-Si sample, suggesting a larger proportion of SiO_2 on the surface. The presence of SiO_2 is larger in PV nano-Si-3h samples than in commercial nano-Si samples. Ball-milled PV nano-Si-3h samples are very reactive to the air and moisture environments because of high surface energy due to the particle size reduction. Hence, ball-milled nano-Si powder is always handled inside a glove box under an argon atmosphere. It is predicted that, somehow, the PV nano-Si-3h sample was exposed to the air during XPS analysis. As a result, it reacted with oxygen and produced a small amount of SiO_2 on the PV nano-Si surface.

Electrochemical performance evaluation

To evaluate the feasibility of the PV nano-Si for application in lithium-ion batteries, cyclic voltammetry (CV) was executed first to understand the lithiation/de-lithiation process among electrodes within the voltage range of 0.01-2.0 V (*vs.* Li/Li^+) at a scan rate of 0.1 mV s^{-1} [Figure 6]. In the CV curves, the first cathodic/anodic scan differs slightly from the second scan, suggesting the SEI layer formation during the first lithiation process which corresponds to irreversible capacity loss[26-28]. All PV nano-Si electrodes show typical lithiation/delithiation processes with a common cathodic peak at around 0.2 V and two common anodic peaks at 0. 3 and 0.5 V which agree with the cathodic/anodic peaks observed in the commercial nano-Si electrode. During discharge, the peak at around 0.2 V corresponds to the Li_xSi_y alloying processes, while two anodic peaks at 0.3 and 0.5 V detected during charge are from the de-alloying processes of the Li_xSi_y phase[29]. However, an obvious anodic peak at around 0.99 V is shown for the PV nano-Si-1h, PV nano-Si-9h, and commercial nano-Si electrodes, suggesting the oxidation of Li_xSi_y (particularly Li_7Si_3) phase back to c-Si[30-31]. The obtained CV results demonstrate that ball-milled PV nano-Si has potential for application in lithium-ion batteries.

To compare storage performance among electrodes, galvanostatic charge-discharge cycling was conducted on CR 2032 coin-type half-cells within a voltage range of 0.01-2.0 V. Figure 7A compares cyclic stability of the ball-milled PV nano-Si electrodes with CMC binder at a 0.03C (1C = 4,200 mA) current rate. The corresponding charge-discharge voltage profiles of the PV nano-Si electrodes with CMC binder are depicted in Figure 7B-D. The measured 1st cycle reversible capacity was 804 mAh g^{-1} for PV nano-Si-1h, 2,366 mAh g^{-1} for PV nano-Si-3h, and 828 mAh g^{-1} for PV nano-Si-9h electrodes, respectively. It is noticeable that the obtained 1st cycle reversible/charge capacity of 2,366 mAh g^{-1} for PV nano-Si-3h electrodes is much higher than that of other electrodes, suggesting that PV nano-Si has potential for lithium-ion battery application. However, the cyclic stability of the PV nano-Si-3h electrode deteriorates similarly to other electrodes, which is a typical nature of silicon anodes. To improve cyclic stability of the PV nano-Si-3h electrode, the CMC binder was modified and the combination of CMC-PAA was used. Figure 7E compares cyclic performance between PV nano-Si-3h and commercial nano-Si electrodes with both CMC binder and modified CMC-PAA binder under the same testing conditions. Indeed, cyclic stability of the PV nano-Si-3h electrode with CMC-PAA binder is improved dramatically with a reversible capacity of 1,005 mAh g^{-1} after 50 cycles whereas it was only 200 mAh g^{-1} with CMC binder. The cyclic performance of the PV nano-Si-3h electrode with CMC-PAA binder is comparable with a commercial nano-Si electrode with CMC-PAA binder. Basically, a silicon anode has a high theoretical specific capacity

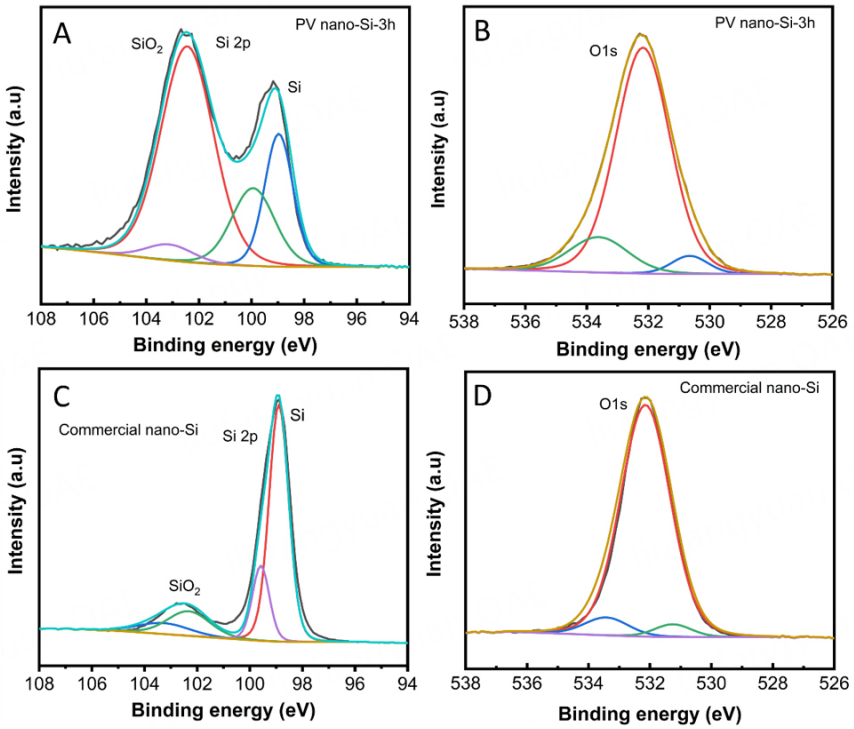

Figure 5. XPS spectra for the core peaks obtained at the surface of the samples: (A and B) Si2p and O1s of the PV nano-Si-3h; and (C and D) Si2p and O1s of the commercial nano-Si powder.

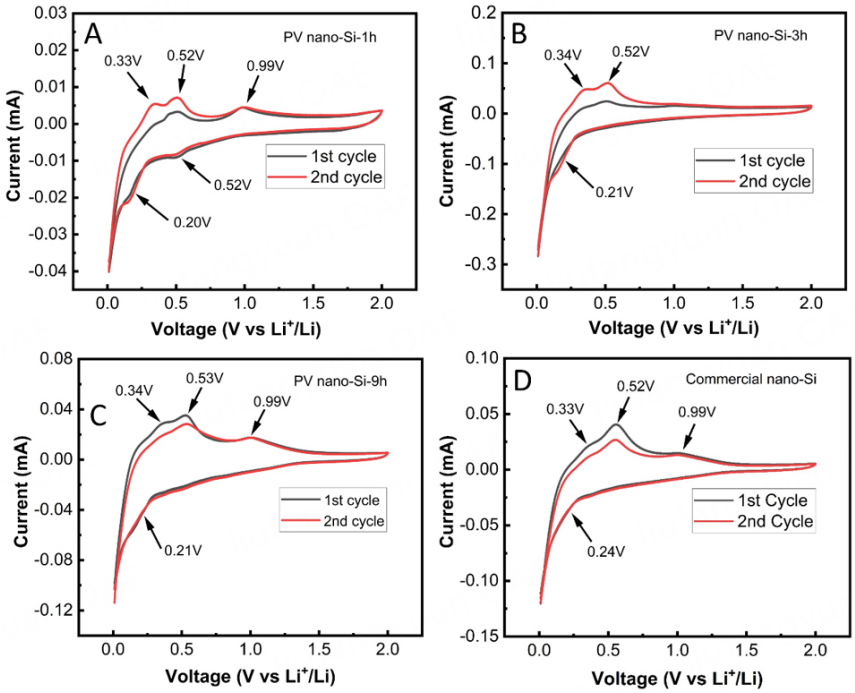

Figure 6. Cyclic voltammetry measurements: (A) PV nano-Si-1h; (B) PV nano-Si-3h; (C) PV nano-Si-9h; and (D) Commercial nano-Si for the first two cycles at a scan rate of 0.1 mV s^{-1}.

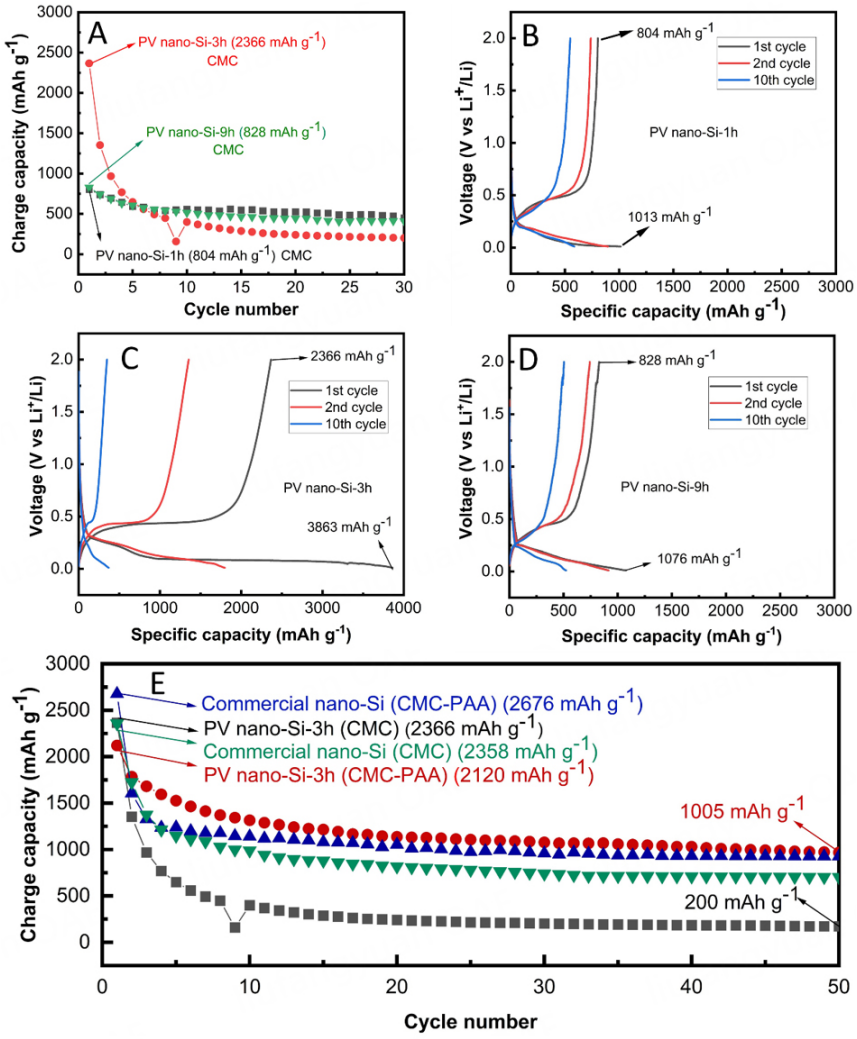

Figure 7. Electrochemical performances: (A) Comparison of cyclic performance among PV nano-Si electrodes (PV nano-Si-1h, PV nano-Si-3h, and PV nano-Si-9h) with CMC binder at 0.03C current rate; (B-D) Corresponding discharge-charge voltage profiles of the PV nano-Si electrodes; and (E) Cyclic performance comparison between PV nano-Si-3h and commercial nano-Si electrodes with CMC-PAA binder at 0.03C current rate.

of 4,200 mAh g^{-1}, ten times larger than a graphite anode (372 mAh g^{-1})[32-34]. Therefore, the current commercial lithium-ion batteries with graphite anodes deliver a low energy density of 200-300 Wh/kg whereas those employing silicon anodes achieve 350-400 Wh/kg. However, lithium-ion batteries with silicon anodes can provide a higher energy density of ~600 Wh/kg or even more if the volume change issue in silicon anodes is minimized properly[35]. It is projected that the PV recycled nano-Si electrode can work the same way as commercial nano-Si anode does.

As binders play a pivotal role in electrode processing for battery technologies, selecting an appropriate binder is essential to achieve high performance batteries[36-38]. To understand the binder effect on the electrochemical performance, a Fourier Transform Infrared Spectroscopy (FTIR) investigation was carried out on CMC, PAA, and a crosslinked CMC-PAA binder [Figure 8]. The FTIR spectrum of a material reveals its chemical environment changes resulting from interactions, typically manifested by shifts towards higher or lower wavenumbers of specific functional group peaks or the emergence of new peaks (or

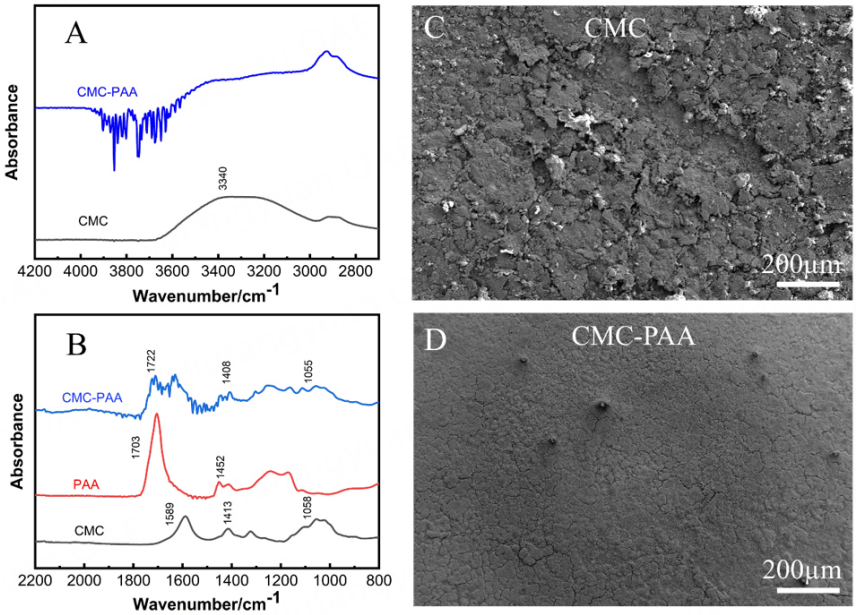

Figure 8. FTIR and post-cycling analysis: (A and B) FTIR characterization of the binders: (A) Comparison between CMC and CMC-PAA at higher wavenumber and (B) Comparison between CMC, PAA, and CMC-PAA at a lower wave number (The crosslinked was formed by heating at 150 °C for 2 h under vacuum); and (C and D) Post-cycling analysis of the electrodes: SEM images of (C) Electrode with CMC binder and (D) Electrode with c-CMC-PAA binder after 200 repeated cycles.

shoulders). The FTIR analysis conducted on the c-PAA-CMC binder revealed a modification in the C = O stretching band of the COOH group in PAA, which shifted from 1,703 cm^{-1} to a series of peaks from 1,630 to 1,722 cm^{-1} [Figure 8B], suggesting the formation of ester groups (COO) due to interchain crosslinking. In addition, the condensation reaction between the OH groups of CMC and COOH groups of PAA is validated by the disappearance of the OH peak in the c-CMC-PAA binder at around 3,340 cm^{-1} [Figure 8A]. It is evidenced that c-CMC-PAA binder has a higher crosslinking density than CMC, which can act to reduce the volume change of the Si particles during cycling. Crosslinked polymers have a higher degree of network connectivity, which has been shown in previous works to restrict Si particle mobility and prevent excessive swelling/shrinking of the electrode, providing better electrochemical performance[37,38]. To support this statement, a post-cycling SEM analysis was conducted on the electrodes after long-term cycling (200 cycles). It is observed that the electrode surface of the c-CMC-PAA binder remains well preserved after repeated cycling [Figure 8D]. In the case of CMC binders, the electrode surface tends to separate from the copper foil current collector due to the swelling/shrinking of the Si particles [Figure 8C], confirming that the c-CMC-PAA binder precludes the expanded Si particles from not escaping from the binder network. As a result, all Si particles with c-CMC-PAA binders contribute to the charge-discharge process delivering high capacity with cycling stability.

CONCLUSIONS

Deconstruction of EoL PV modules and subsequent Si separation without any cross-contamination are a serious challenge to reusing the recovered Si for new applications. Even more challenges are realized for purifying the recovered PV Si with both high purity and yield. In this study, an environmentally sustainable process, including recycling and subsequent purification, is developed to effectively manage PV waste and maintain high yield recovery with high purity of the Si. An acid mixture of HNO_3-H_3PO_4 was found to be an effective solvent for purification to achieve high-purity and high-quality Si. The demonstrated time-dependent ball milling technique is critical to producing high-quality PV nano-Si with required properties

(high purity, high crystallinity, and distinct morphology) which are comparable with commercially available nano-Si. To make this PV nano-Si viable, a facile in-situ thermal-crosslinking technique is used to achieve high strength binders by incorporating CMC and PAA precursors. The obtained binder can enhance cycling performance of the silicon anode. This study provides a technology to develop high performance Si-based, low-cost lithium-ion batteries made of waste resources. Even though the technology has been validated in a laboratory scale, large-scale purification of PV cells is quite a challenge because this step requires basic and acidic dissolution which will produce a huge amount of heat due to exothermic reaction. From the safety point of view, a dedicated chemical reactor is required to control all parameters for large-scale silicon production.

DECLARATIONS

Acknowledgments

The authors acknowledge the support from Deakin Advanced Characterization Facilities.

Authors' contributions

Methodology, characterization, writing - original draft: Nelson A
Characterization: Sharma N, Han Q
Characterization, supervision, writing - review & editing: Mateti S
Conceptualization, supervision, review & editing: Chen Y
Conceptualization, supervision, methodology, project management, writing - original draft, review & editing: Rahman MM

Availability of data and materials

Not applicable.

Financial support and sponsorship

This work is supported by an HDR scholarship through Deakin University Postgraduate Research (DUPR) allocation (Code: NPMR07) and financial assistance from the ARC-Industrial Transformation Research Hub (IH200100035).

Conflicts of interest

All authors declared that there are no conflicts of interest.

Ethical approval and consent to participate

Not applicable.

Consent for publication

Not applicable.

REFERENCES

1. Avril S, Mansilla C, Busson M, Lemaire T. Photovoltaic energy policy: financial estimation and performance comparison of the public support in five representative countries. *Energy Policy* 2012;51:244-58. DOI
2. Fthenakis VM, Kim HC, Alsema E. Emissions from photovoltaic life cycles. *Environ Sci Technol* 2008;42:2168-74. DOI PubMed
3. Cheng J, Yeh C, Tu C. Trust and knowledge sharing in green supply chains. *Int J Supply Chain Manag* 2008;13:283-95. DOI
4. Chowdhury M, Shahahmadi S, Chelvanathan P, et al. Effect of deep-level defect density of the absorber layer and n/i interface in perovskite solar cells by SCAPS-1D. *Results Phys* 2020;16:102839. DOI

5. Deng R, Chang NL, Ouyang Z, Chong CM. A techno-economic review of silicon photovoltaic module recycling. *Renew Sust Energy Rev* 2019;109:532-50. DOI
6. Dias P, Javimczik S, Benevit M, Veit H. Recycling WEEE: polymer characterization and pyrolysis study for waste of crystalline silicon photovoltaic modules. *Waste Manag* 2017;60:716-22. DOI PubMed
7. Gholami A, Ameri M, Zandi M, Ghoachani RG, Pierfederici S, Kazem HA. Step-by-step guide to model photovoltaic panels: an up-to-date comparative review study. *IEEE J Photovoltaics* 2022;12:915-28. DOI
8. Giacchetta G, Leporini M, Marchetti B. Evaluation of the environmental benefits of new high value process for the management of the end of life of thin film photovoltaic modules. *J Clean Prod* 2013;51:214-24. DOI
9. Mahmoudi S, Huda N, Behnia M. Environmental impacts and economic feasibility of end of life photovoltaic panels in Australia: a comprehensive assessment. *J Clean Prod* 2020;260:120996. DOI
10. Kang S, Yoo S, Lee J, Boo B, Ryu H. Experimental investigations for recycling of silicon and glass from waste photovoltaic modules. *Renew Energy* 2012;47:152-9. DOI
11. Chung J, Seo B, Lee J, Kim JY. Comparative analysis of I_2-KI and HNO_3 leaching in a life cycle perspective: towards sustainable recycling of end-of-life c-Si PV panel. *J Hazard Mater* 2021;404:123989. DOI
12. Singh JK, Molinari G, Bui J, Soltani B, Rajarathnam GP, Abbas A. Life cycle assessment of disposed and recycled end-of-life photovoltaic panels in Australia. *Sustainability* 2021;13:11025. DOI
13. Latunussa CE, Ardente F, Blengini GA, Mancini L. Life cycle assessment of an innovative recycling process for crystalline silicon photovoltaic panels. *Solar Energy Mater Solar Cells* 2016;156:101-11. DOI
14. Huang W, Shin WJ, Wang L, Sun W, Tao M. Strategy and technology to recycle wafer-silicon solar modules. *Solar Energy* 2017;144:22-31. DOI
15. Klugmann-radziemska E, Ostrowski P. Chemical treatment of crystalline silicon solar cells as a method of recovering pure silicon from photovoltaic modules. *Renew Energy* 2010;35:1751-9. DOI
16. Klugmann-radziemska E, Ostrowski P, Drabczyk K, Panek P, Szkodo M. Experimental validation of crystalline silicon solar cells recycling by thermal and chemical methods. *Solar Energy Mater Solar Cells* 2010;94:2275-82. DOI
17. Lawson AC, Larson AC, Aronson MC, et al. Magnetic and crystallographic order in α-manganese. *J Appl Phys* 1994;76:7049-51. DOI
18. Toby BH. *EXPGUI*, a graphical user interface for *GSAS*. *J Appl Cryst* 2001;34:210-3. DOI
19. Joseph T, White D. Understanding the role of concentrated phosphoric acid solutions as high-temperature silicon nitride etchants. *ECS J Solid State Sci Technol* 2021;10:024006. DOI
20. Sundaram K, Sah R, Baumann H, Balachandran K, Todi R. Wet etching studies of silicon nitride thin films deposited by electron cyclotron resonance (ECR) plasma enhanced chemical vapor deposition. *Microelectron Eng* 2003;70:109-14. DOI
21. Gelder W, Hauser VE. The etching of silicon nitride in phosphoric acid with silicon dioxide as a mask. *J Electrochem Soc* 1967;114:869. DOI
22. Radvanyi E, De Vito E, Porcher W, Larbi SJS. An XPS/AES comparative study of the surface behaviour of nano-silicon anodes for Li-ion batteries. *J Anal At Spectrom* 2014;29:1120-31. DOI
23. Philippe B, Dedryvère R, Allouche J, et al. Nanosilicon electrodes for lithium-ion batteries: interfacial mechanisms studied by hard and soft X-ray photoelectron spectroscopy. *Chem Mater* 2012;24:1107-15. DOI
24. Franklin GE, Rich DH, Hong H, Miller T, Chiang T. Interface formation and growth of InSb on Si_{100}. *Phys Rev B Condens Matter* 1992;45:3426-34. DOI PubMed
25. Cros A, Saoudi R, Hollinger G, Hewett CA, Lau SS. An x-ray photoemission spectroscopy investigation of oxides grown on Au x Si_{1-x} layers. *J Appl Phys* 1990;67:1826-30. DOI
26. Rahman MM, Mateti S, Sultana I, et al. End-of-life photovoltaic recycled silicon: a sustainable circular materials source for electronic industries. *Adv Energy Sustain Res* 2021;2:2100081. DOI
27. Li J, Dudney NJ, Nanda J, Liang C. Artificial solid electrolyte interphase to address the electrochemical degradation of silicon electrodes. *ACS Appl Mater Interfaces* 2014;6:10083-8. DOI PubMed
28. Li M, Hou X, Sha Y, et al. Facile spray-drying/pyrolysis synthesis of core-shell structure graphite/silicon-porous carbon composite as a superior anode for Li-ion batteries. *J Power Sources* 2014;248:721-8. DOI
29. Liu N, Liu J, Jia D, et al. Multi-core yolk-shell like mesoporous double carbon-coated silicon nanoparticles as anode materials for lithium-ion batteries. *Energy Storage Mater* 2019;18:165-73. DOI
30. Kasavajjula U, Wang C, Appleby AJ. Nano- and bulk-silicon-based insertion anodes for lithium-ion secondary cells. *J Power Sources* 2007;163:1003-39. DOI
31. Obrovac MN, Krause LJ. Reversible cycling of crystalline silicon powder. *J Electrochem Soc* 2007;154:A103. DOI
32. Wang M, Wang G, Wang S, et al. In situ catalytic growth 3D multi-layers graphene sheets coated nano-silicon anode for high performance lithium-ion batteries. *Chem Eng J* 2019;356:895-903. DOI
33. Xing Y, Zhang L, Mao S, et al. Core-shell structure of porous silicon with nitrogen-doped carbon layer for lithium-ion batteries. *Mater Res Bull* 2018;108:170-5. DOI
34. Tranchot A, Etiemble A, Thivel P, Idrissi H, Roué L. In-situ acoustic emission study of Si-based electrodes for Li-ion batteries. *J Power Sources* 2015;279:259-66. DOI
35. Cleantech insights-Materials & Chemicals, 30 March 2023. Silicon anodes can improve EV battery density and extend range without cost increase. Available from: https://www.cleantech.com/silicon-anodes-can-improve-ev-battery-density-and-extend-range-without-

cost-increase/ [Last accessed on 9 May 2024].

36. Su H, Fu C, Zhao Y, et al. Polycation binders: an effective approach toward lithium polysulfide sequestration in Li-S Batteries. *ACS Energy Lett* 2017;2:2591-7. DOI
37. Koo B, Kim H, Cho Y, Lee KT, Choi N, Cho J. A highly cross-linked polymeric binder for high-performance silicon negative electrodes in lithium ion batteries. *Angew Chem Int Ed* 2012;124:8892-7. DOI
38. Hu X, Liang K, Li J, Ren Y. A highly crosslinked polymeric binder for silicon anode in lithium-ion batteries. *Mater Today Commun* 2021;28:102530. DOI